

## Accepted Manuscript

Characterization of the Low Latitude Plasma Density Irregularities Observed using C/NOFS and SCINDA Data

Geoffrey Andima, Emirant B. Amabayo, Edward Jurua, Pierre J. Cilliers

PII: S0273-1177(17)30578-1

DOI: <http://dx.doi.org/10.1016/j.asr.2017.08.003>

Reference: JASR 13359

To appear in: *Advances in Space Research*

Received Date: 4 April 2017

Accepted Date: 4 August 2017



Please cite this article as: Andima, G., Amabayo, E.B., Jurua, E., Cilliers, P.J., Characterization of the Low Latitude Plasma Density Irregularities Observed using C/NOFS and SCINDA Data, *Advances in Space Research* (2017), doi: <http://dx.doi.org/10.1016/j.asr.2017.08.003>

This is a PDF file of an unedited manuscript that has been accepted for publication. As a service to our customers we are providing this early version of the manuscript. The manuscript will undergo copyediting, typesetting, and review of the resulting proof before it is published in its final form. Please note that during the production process errors may be discovered which could affect the content, and all legal disclaimers that apply to the journal pertain.

# Characterization of the Low Latitude Plasma Density Irregularities Observed using C/NOFS and SCINDA Data

Geoffrey Andima<sup>a,\*</sup>, Emirant B Amabayo<sup>a,b</sup>, Edward Jurua<sup>a</sup>, Pierre J Cilliers<sup>c</sup>

<sup>a</sup>*Department of Physics, Mbarara University of Science and Technology, Mbarara, Uganda*

<sup>b</sup>*Department of Physics, Busitema University, Tororo, Uganda*

<sup>c</sup>*South African National Space Agency (SANSA) Space Science, Hermanus, South Africa*

---

## Abstract

Complex electrodynamic processes over the low latitude region often result in post sunset plasma density irregularities which degrade satellite communication and navigation. In order to forecast the density irregularities, their occurrence time, duration and location need to be quantified. Data from the Communication/Navigation Outage Forecasting System (C/NOFS) satellite was used to characterize the low latitude ion density irregularities from 2011 to 2013. This was supported by ground based data from the SCIntillation Network Decision Aid (SCINDA) receivers at Makerere (Geographic coordinate 32.6°E, 0.3°N, and dip latitude -9.3°N) and Nairobi (Geographic coordinate 36.8°E, -1.3°N, and dip latitude -10.8°N). The results show that irregularities in ion density have a daily pattern with peaks from 20:00-24:00 Local Time (LT). Scintillation activity at L band and VHF over East Africa peaked in 2011 and 2012 from 20:00-24:00 LT, though in many cases scintillation at VHF persisted longer than that at L band. A longitudinal pattern in ion density irregularity occurrence was observed with peaks over 135-180°E and 270-300°E. The likelihood of ion density irregularity occurrence decreased with increasing altitude. Analysis of C/NOFS zonal ion drift velocities showed that the largest nighttime and daytime drifts were in 270-300°E and 300-330°E longitude regions respectively. Zonal irregularity drift velocities over East Africa were for the first time estimated from L-band scintillation indices. The results show that the velocity of plasma density irregularities in 2011 and 2012 varied daily, and hourly in the range of 50-150 m s<sup>-1</sup>. The zonal drift velocity estimates from the L-band scintillation indices had good positive correlation with the zonal drift velocities derived from VHF receivers by the spaced receiver technique.

*Key words:* Zonal ion drifts, Ionospheric scintillations, Low latitude irregularities

---

## 1. Introduction

The post sunset low latitude ionosphere is often characterized by large scale density depletions relative to the background plasma, often referred to as Plasma Bubbles (PBs). The depletions are normally initiated from the bottom of the F region; they evolve primarily by Rayleigh Taylor instability mechanism (Kelley, 2009), and then rise to higher altitudes. Steep density gradients exist between the walls of the depletions and the ambient plasma, and this creates favorable conditions for the onset of secondary instability processes responsible for the formation of smaller irregularities (Haerendel, 1973). These small scale irregularities (typical of the order of first Fresnel radius) are responsible for producing scintillations in transionospheric radio waves (Yeh and Liu, 1982). In addition to the irregularity scale sizes, the characteristics of the scintillations produced on transionospheric radio links depend on the Ionospheric Pierce

---

\*Corresponding author

*Email address:* geoffrey.andima@gmail.com (Geoffrey Andima)

Point (IPP) velocity, and the general motion of the ionosphere (Kintner *et al.*, 2004). The ionosphere exhibits Local Time (LT) dependent motions controlled by different electrodynamic processes. The vertical plasma motions are driven by the E and F region dynamo processes which dominate during the daytime and nighttime respectively. The horizontal plasma motions are modulated by zonal neutral winds. The neutral winds in the F region interact with the magnetic fields to produce a vertical polarization electric field which moves the plasma in east-west direction with velocities nearly equal to that of the neutral winds (Richmond and Roble, 1997). The motion of the plasma transverse to the magnetic field generates a damping force through collision between the ions and the neutral particles (atoms and molecules). This force is reduced in the depleted regions, and the ions in the depleted regions are accelerated to drift with velocities higher than the general velocity of the ambient plasma.

The zonal ion motions have been extensively studied using both ground based data (Fejer *et al.*, 1985, 1991; Ji *et al.*, 2011) and in-situ data (Jensen and Fejer, 2007; Huang *et al.*, 2010; Fejer *et al.*, 2013). A common observation from these studies is that the daytime drifts are westward while the nighttime drifts are eastward. The magnitude of the nighttime drifts maximize just before local midnight. However, longitudinal imbalances in plasma drifts have been observed where the largest nighttime drifts are in the American longitude sector (Fejer *et al.*, 2013; Coley *et al.*, 2014). The longitudinal differences suggest possible differences in the thermospheric winds responsible for the quiet time zonal plasma drifts. In a bid to forecast the time evolution of scintillation, characterizing the zonal plasma motions, especially that of large plasma depletions becomes a prerequisite.

A conventional approach to estimate the zonal drift velocities of equatorial irregularities is the spaced receiver technique (Ledvina *et al.*, 2004). This technique is based on estimating the diffraction pattern velocity by cross correlating the received power fluctuations from the same satellite at two Very High Frequency (VHF) or L band antennas in an east-west alignment. Olwendo *et al.* (2013) estimated the zonal irregularity drifts over Kenya using the VHF receiver at Nairobi (Geographic coordinate 36.8°E, -1.3°N, and dip latitude -10.8°N), and reported irregularity drift velocities of about 30-160 m s<sup>-1</sup>. Complementary research over the same region still remains limited, probably due to the few VHF receivers over the region. Alternative methods to estimate the zonal irregularity drift velocities have been explored. For instance nighttime imagers (Immel *et al.*, 2004; Nade *et al.*, 2013) and recently scintillation indices (Carrano *et al.*, 2016) have proved to be reliable in inferring the low latitude zonal irregularity drift velocities.

The Communication/Navigation Outage Forecasting System (C/NOFS) satellite was the first to be dedicated to radio wave scintillation and ionospheric irregularity forecasting (Beaujardière *et al.*, 2004). The C/NOFS satellite was launched in an elliptical orbit with inclination 13 degrees, and initial perigee 400 km and apogee 850 km. To maximize its capabilities, the satellite had on board a number of sensors (e.g. retarding potential analyzer (RPA), ion drift meter (IDM)) and other instruments (e.g. Planar Langmuir Probe (PLP), Vector Electric Field Instrument (VEFI)) to measure different neutral and ionospheric parameters. The Ion Velocity Meter (IVM), which was part of the Coupled Ion Neutral Dynamics Investigation (CINDI) package comprised of the RPA to measure ion temperature, ion composition and ion velocity in the satellite direction, and the IDM measures the vertical and meridional ion velocities. Detailed description of C/NOFS mission and the different instruments which were on board can be found in earlier publications (e.g. Beaujardière *et al.* 2004; Stoneback *et al.* 2011; Fejer *et al.* 2013; Coley *et al.* 2014). Quite a large volume of the drift velocity data recorded by the IVM before the demise of C/NOFS satellite in November 2015 has been analyzed, and this has provided a wealth of information on the low latitude climatology of the meridional (Rodrigues *et al.*, 2011; Stoneback *et al.*, 2011) and the zonal (Coley *et al.*, 2014) ion drifts. In this paper, the low latitude global statistics of irregularity occurrence using data from C/NOFS satellite

are presented in section 3.1. The local time and seasonal variations of the zonal ion drift velocities from C/NOFS satellite are discussed in section 3.2. The last section analyzes the zonal irregularity drift velocities over the East African region.

## 2. Experimentation and Analysis

In-situ data from C/NOFS satellite are publicly available in the common data format (cdf). The cdf files used in this study were obtained from the space physics data facility website<sup>1</sup> maintained by National Aeronautics Space Agency (NASA). Available on this website are software packages to extract the readable files from the cdf files. We used the MATLAB compatible software package to extract the ion density and ion drift velocities from the IVM for the period 2011-2013. The ion drift velocities were converted from the satellite frame of reference to the magnetic coordinates using the International Geomagnetic Reference Field (IGRF) model. Spurious data points were minimized by using 10 seconds running averages of the quiet time 1 second ion drift velocities in magnetic east-west direction. The ten-second window was chosen for comparison with Fejer *et al.* (2013)

The RPA measurements of in-situ ion density have previously been used to identify plasma irregularities (Kil and Heelis, 1998; Su *et al.*, 2006; Liu *et al.*, 2012). We followed the approach of Su *et al.* (2006) to calculate the ion density fluctuations  $\delta_{ion}$ , using the Equation

$$\delta_{ion} = \frac{\left[ \frac{1}{10} \sum_{n=1}^{10} (\log N_i - \log N_{oi})^2 \right]^{\frac{1}{2}}}{\frac{1}{10} \sum_{n=1}^{10} \log N_{oi}}, \quad (1)$$

where  $N_i$  and  $N_{oi}$  are the  $i^{th}$  time series data values for the measured and the linearly fitted ion densities respectively. In our search algorithm, an irregularity is flagged on when  $\delta_{ion}$  exceeds a predetermined threshold, and the irregularity terminated if  $\delta_{ion}$  falls below the set threshold. In this study, we determined the threshold by first generating time series ion density and  $\delta_{ion}$  plots for some selected test cases. Based on these plots and to be consistent with Su *et al.* (2006), we adopted  $\delta_{ion} \geq 0.3\%$  as the threshold to identify the irregularities in the ion density. Short noise effects were minimized by requiring that at least four consecutive values of  $\delta_{ion}$  should exceed the threshold. It should be noted that cases of the satellite encountering the same irregularity especially in different orbits were possible since an irregularity may last for hours.

In addition to the C/NOFS satellite data, the Air Force Research Laboratory (AFRL) in coordination with Boston College, USA, have installed a system of ground based GPS receivers to provide complementary data for C/NOFS mission. Table 1 gives a summary of the coordinates of the ground receivers from which data used in this study were obtained. The public domain software developed by GPS Silicon Valley, **parseismr.exe**, was used to obtain the standard deviation  $\sigma_\phi$ , of the phase measurements, and the normalized standard deviation  $S_4$ , of the signal power from the 60 s data. Multi path effects were minimized by considering data for satellites at higher elevation angles ( $\geq 30^\circ$ ).

Under weak scatter assumption (Rino, 1979), the irregularity drift velocity  $V_d$ , may be estimated from the satellite scan velocity and propagation geometry (Carrano *et al.*, 2016) using the Equation

$$V_d = V_y + \frac{(V_x \sin \psi - V_z \cos \psi) \sin \phi \tan \theta}{\cos \psi - \cos \phi \sin \psi \tan \theta} \pm \sqrt{1 + \frac{\sin^2 \phi \tan^2 \theta}{(\cos \psi - \cos \phi \sin \psi \tan \theta)^2} \frac{F_s}{\tau} Q_\sigma \left[ \frac{\sigma_\phi}{S_4} \right]^{\frac{2}{p-1}}}, \quad (2)$$

<sup>1</sup><http://spdf.gsfc.nasa.gov>

Table 1: The locations of the ground GPS in fracture from which data used in this study was obtained

Station			Geographic		Geomagnetic	
Place	Type	Code	Lon (°E)	Lat (°N)	Lon (°E)	Lat (°N)
Makerere	GPS-SCINDA	MAK	32.6	0.3	104.2	-9.3
Makerere	VHF-SCINDA	VHF	32.6	0.3	104.2	-9.3
Nairobi	GPS-SCINDA	UON	36.8	-1.3	108.5	-10.7
Nairobi	VHF-SCINDA	VHF	36.8	-1.3	108.5	-10.7

where  $V_y$ ,  $V_x$  and  $V_z$  are the IPP velocities in the magnetic east, north and upward directions.  $\phi$ ,  $\psi$  and  $\theta$  are the magnetic azimuth, dip and propagation (nadir) angles at the IPP respectively. The phase detrend filter cut off  $f_c$  ( $f_c = \frac{1}{\tau}$ ) is 0.1 Hz (Van Dierendonck *et al.*, 1993) for the Novatel GPS-SCINDA models used in this study. We adapted Equation 2 to estimate the zonal velocity of irregularities. The Fresnel radius  $F_s$  was estimated by assuming the irregularity layer altitude  $z$  to be 350 km, and wavelength  $\lambda$  for GPS L1 frequency. The parameter  $Q_\sigma$  in Equation 2 depends only on the phase spectral index  $\rho$  (Carrano *et al.*, 2016), and it is expressed as

$$Q_\sigma = \left[ \frac{2^{(\rho+1)/2} \pi^{\rho-1/2} \Gamma(5/4 - \rho/4)}{\Gamma(1/4 + \rho/4)} \right]^{\frac{1}{\rho-1}}, \quad (3)$$

where  $\Gamma$  is Euler's gamma function. De Kamp and Cannon (2009) estimated the spectral index of irregularities by analyzing 1 s TEC data over 17 min interval. In this study, the spectral index was estimated from the 1 s ion density data using Fast Fourier Transform (FFT). Rino (1979) noted that, the in-situ spectral index is one less than the three dimensional phase spectral index  $\rho$ , in Equation 3. We therefore added one to our estimates of spectral index from the in-situ data to obtain the phase spectral index  $\rho$ .

### 3. Results and discussions

#### 3.1. Statistics of ion density irregularities

The global low latitude irregularity occurrence statistics using in-situ measurements had been presented before (e.g. Kil and Heelis 1998; Su *et al.* 2006). In this paper we seek to extend these statistics using C/NOFS's ion density data. To identify irregularities, we first determined the ion density fluctuations using Equation 1. An irregularity was said to have occurred if the value of  $\delta_{ion}$  exceeded 0.3%. Figure 1 shows how well the ion density fluctuations captured the irregularities in the ion density. From Figure 1 a, ion density irregularities were detected by C/NOFS satellite during orbit 18358 between 21-39°E from 20:30-21:40 LT on 2011-09-03. During this time, the altitude of the satellite was between 647 and 703 km, and this shows that the ion density irregularities were in the topside ionosphere. In the next orbit (18359), ion density irregularities were again encountered by the satellite in the same longitude sector from about 22:00-23:24 LT in the altitude range of about 613-556 km (Figure 1 b). In Figure 1 c and d, the ion density irregularities encountered by C/NOFS satellite on 2012-03-21 over 27-42°E longitude sectors in two orbits are shown. When in orbit 21346, the satellite detected ion density irregularities between 36-40°E from 21:30-21:45 LT. In about 1.8 hours later, the satellite was over the same region, and encountered several ion density irregularities from about 22:30-23:15 LT (Figure 1 d). The satellite track at the moment it observed the ion density irregularities in Figure 1 b and L band amplitude scintillations observed on some selected GPS satellite links on the same day are shown in Figure 2. From Figure 2, C/NOFS satellite entered

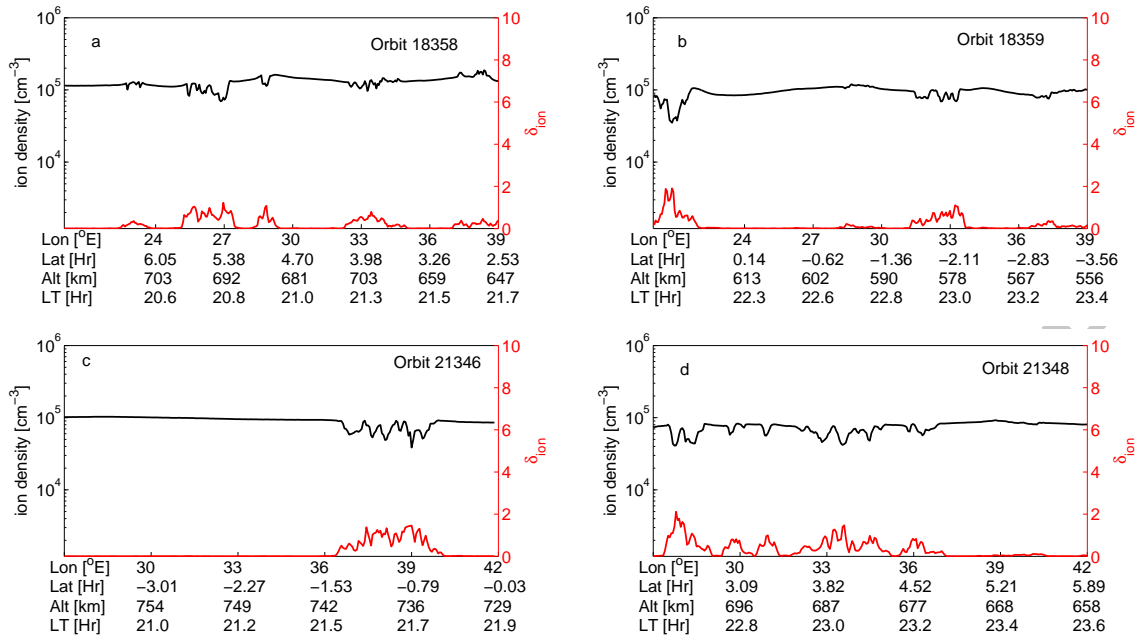


Figure 1: Ion density irregularities for selected orbits on 2011-09-03 (a and b) and 2012-03-21 (c and d)

density irregularities from 22:52-22:58 LT, and just minutes later, strong amplitude scintillation ( $S_4 \geq 0.4$ ) of signals from PRN 6 were observed from 23:00-23:15 LT about the same position where C/NOFS satellite entered the density irregularities. On the same evening, PRN 16 was moving southwards and signals from it started scintillating strongly at about 22:15-22:45 LT, about the same time when the satellite entered the density irregularities. Based on these observations, there could be a possible relationship between the density irregularities observed by the C/NOFS satellite and those from ground measurements.

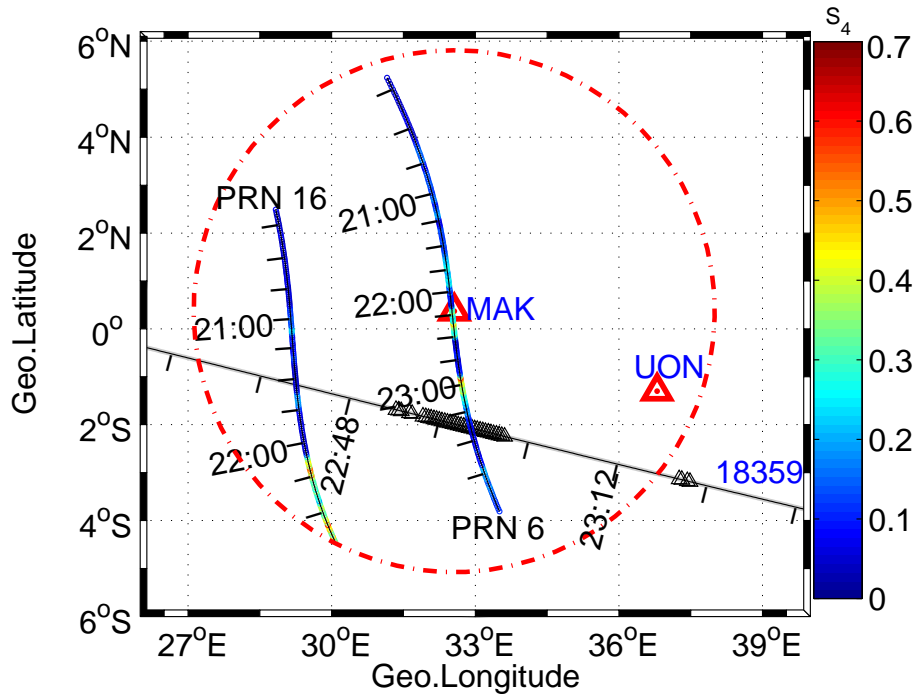


Figure 2: Ground projection of the trajectory of the C/NOFS satellite orbit 18359 on 2011-09-03. The black spots on the satellite tracks indicate points where the irregularities were encountered. The circle is a projection of the 30° elevation centered at MAK indicating regions in which scintillations were observed. Also shown on the tracks are the local times

### 3.1.1. Diurnal variation of ion density irregularities

To study the variations in the occurrence of the low latitude ion density irregularities, we have analyzed the 1 s IVM ion density data. The fluctuations in ion density for the apex altitude range 400-1000 km for satellite passes over East Africa were determined using Equation 1. The diurnal variations of the ion density irregularities together with amplitude scintillations from MAK and UON GPS-SCINDA receivers in 2011 and 2012 are shown in Figure 3. 2013 was not included due to data paucity from the SCINDA receivers. For the scintillation statistics, an event was defined by  $S_4$  exceeding a background noise level of 0.1 for satellites of elevation greater than  $30^\circ$ . The occurrence probabilities were then computed by expressing the number of events as a fraction of the total number of observations.

Figure 3 shows that both the ion density irregularities and scintillation activity over East Africa had the highest likelihood of occurrence between 20:00-00:00 LT in 2011 and 2012. The occurrence probabilities decreased gradually from midnight to the morning terminator. The rate of decrease was faster for scintillation activity than for ion density irregularity occurrence. This could be due to the rapid post midnight decay of the small scale irregularities which are responsible for L band scintillations (Rao *et al.*, 2005). The decrease in the likelihood of occurrence after midnight is probably as a consequence of decreased electrodynamic processes responsible for irregularity formation.

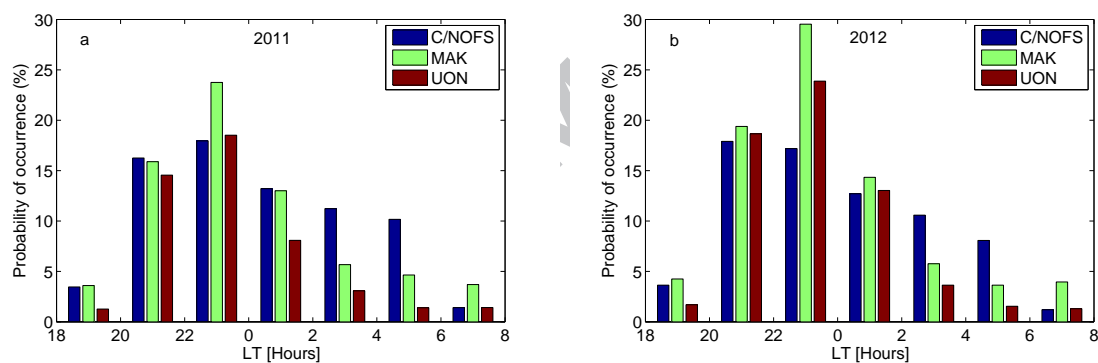


Figure 3: C/NOFS observations of diurnal variation of the low latitude ion density irregularities compared with terrestrial observations of amplitude scintillation from MAK and UON

### 3.1.2. Longitudinal variations of ion density irregularities

The longitudinal variation of ion density irregularity occurrence is shown in Figure 4. The greatest probability of irregularity occurrence was observed at about  $270\text{-}300^\circ\text{E}$  followed by  $135\text{-}180^\circ\text{E}$  and  $0\text{-}30^\circ\text{E}$  longitude sectors. The longitudes  $150\text{-}180^\circ\text{E}$  and  $270\text{-}330^\circ\text{E}$  correspond to regions of positive and negative magnetic declinations respectively. This confirms the fact that declination angle is an important factor in plasma density irregularity formation (Abdu *et al.*, 1981; Maruyama and Matuura, 1984; Kil and Heelis, 1998). The importance arises from the role played by the seasonally dependent thermospheric neutral winds of which the effects at the magnetic meridian are influenced by the magnetic declination. Burrell *et al.* (2012) observed that, in regions of positive (negative) declinations, the northward (southward) field aligned drifts are strongest between 17:30-21:30 LT, and they pointed out neutral winds as the largest contributor to these drifts. The field aligned drifts result in zonal and vertical polarization electric fields. After sunset, the vertical plasma motions resulting from the zonal polarization electric field (Heelis, 2004) raises the F layer into regions of low chemical loss. This may result in increased amplitude of the prereversal polarization electric field, an important factor in irregularity development. Transequatorial flow of neutral wind also has a notable effect on irregularity occurrence (Maruyama and Matuura, 1984). Kil and Heelis (1998) attributed

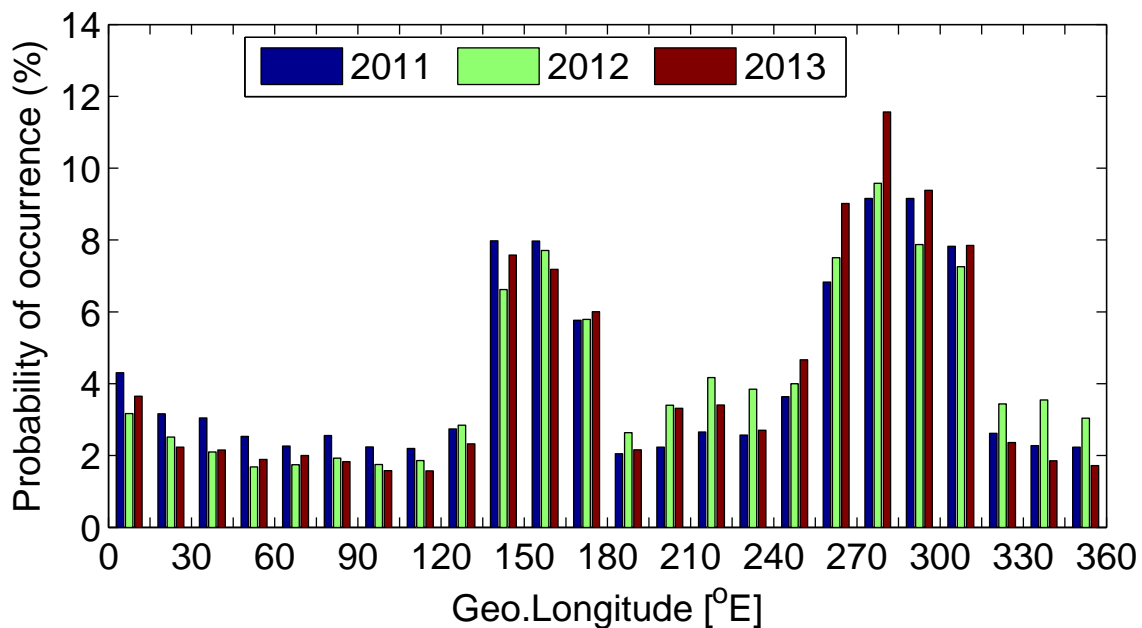


Figure 4: Longitudinal variation of ion density irregularities for 2011, 2012 and 2013.

the low probabilities of irregularity occurrence they observed from 180-270°E to large inter-hemispheric neutral winds in this longitude sector which might have produced a suppression effect on the growth rate of irregularities during the different seasons.

### 3.1.3. Variation of ion density irregularities with altitude

The altitude variation of the orbital path of C/NOFS satellite provided a great opportunity to infer the most active altitude regions for irregularity formation. We have studied the distribution of the ion density irregularities with altitude and the results are shown in Figure 5. The occurrence probabilities indicated were deduced by first binning the satellite tracks according to altitude (200 km bin size) and LT (2 h bin size). The number of ion density irregularities in a given bin were then expressed as a fraction of the satellite passes in that bin. Figure 5 shows that most of the ion density irregularities occurred within 400-600 km. The likelihood of occurrence of plasma density irregularities decreased with increase in altitude. This trend was exhibited from 2011-2013 (Figure 5 a, b and c). A possible explanation for the high probabilities at lower altitudes is that in some cases, the intermediate scale irregularities generated from the bottomside irregularities might have failed to propagate into the topside ionosphere (Hysell and Burcham, 1998).

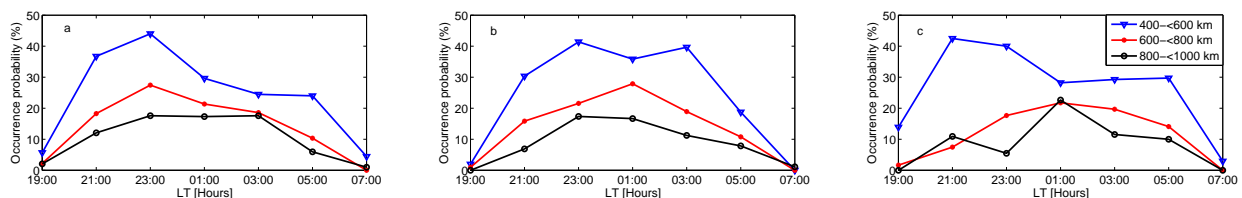


Figure 5: Variation of irregularity occurrence with altitude for 2011 (a), 2012 (b) and 2013 (c).

### 3.2. Zonal ion drift climatology

Zonal ion drifts are indicative of the thermospheric neutral winds which to a large extent originate from the lower atmosphere (Richmond and Roble, 1997). Therefore zonal ion drifts are important in understanding the coupling processes between the lower and upper atmosphere.

The seasonal and local time variations of the zonal ion drifts are shown in Figure 6. The drifts shown were obtained by averaging the 1 second IVM data for the geomagnetic latitude range  $\pm 8^\circ\text{N}$  binned at 20 minutes. From Figure 6, it can be observed that the ions drift

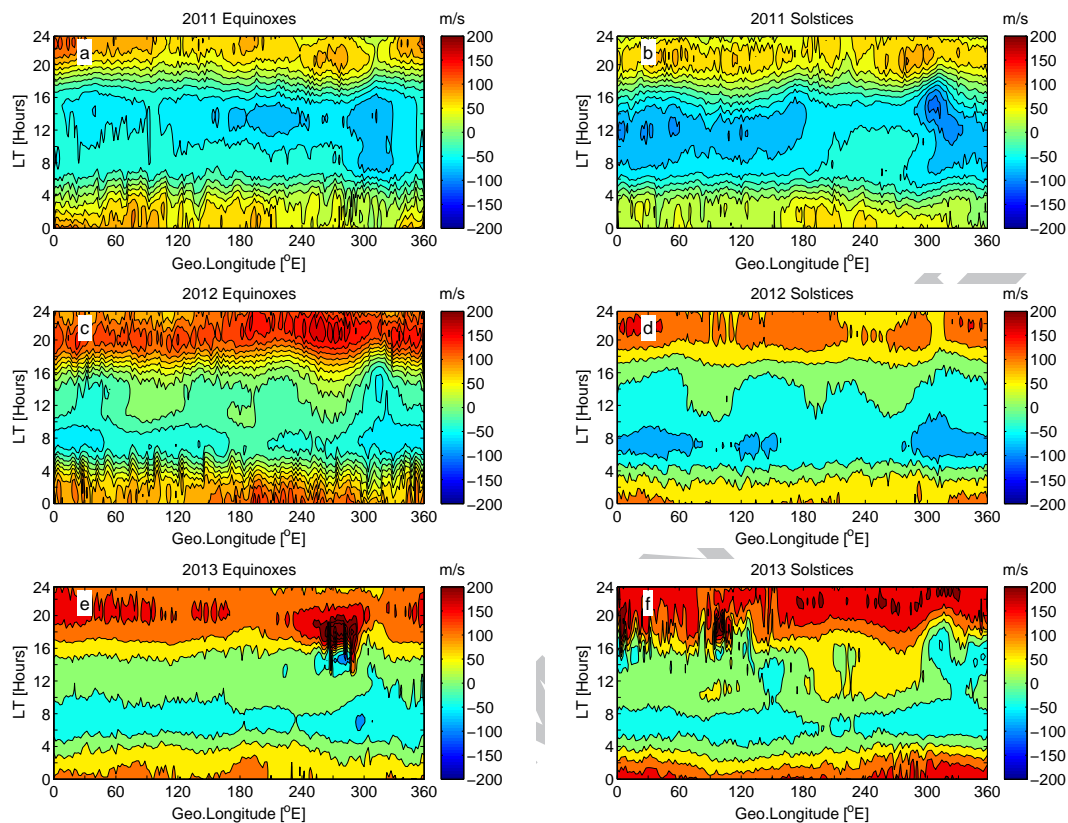


Figure 6: Zonal ion drifts for 2011, 2012 and 2013 from the IVM data. In these plots, eastward drifts are marked positive and the westward drifts are negative

westward during the day, and this is reversed at night. The magnitude of the nighttime ion drifts during the equinox months were generally higher than those during the solstices. The drifts were observed to be longitude depended, with the longitude range  $300\text{-}330^\circ\text{E}$  having the largest daytime drifts (Figure 6 a, b, d and e). The largest nighttime drifts were observed in the longitude range  $270\text{-}300^\circ\text{E}$  followed by  $0\text{-}30^\circ\text{E}$ . The magnitude of the daytime peaks were smaller in 2013 than in 2011 while the reverse was true for the nighttime peaks. The reduced ion damping during lower solar activity years is a possible explanation for the higher amplitude of the daytime peaks in 2011. Fejer *et al.* (2013) using VEFI measurements within  $\pm 5^\circ\text{N}$  of the magnetic equator observed similar results with the largest eastward drifts in  $240\text{-}300^\circ\text{E}$  and smallest westward drift in  $180\text{-}210^\circ\text{E}$  longitude sectors. Coley and Heelis (1994) observed that both neutrals and ions have about the same zonal drift velocity at night, an indication that the nighttime zonal ion drifts may be used as a proxy for the zonal drift velocity of the neutral winds (Heelis, 2004). If so, the large nighttime zonal ion drift velocities observed in the longitude  $270\text{-}300^\circ\text{E}$  and  $0\text{-}30^\circ\text{E}$  imply that large zonal neutral wind velocities exist in these longitudes. Therefore the high likelihood of occurrence of density irregularities in these longitudes may partly be through a wind driven mechanism.

### 3.3. Irregularity zonal drift velocities over East Africa

#### 3.3.1. Irregularity spectral index

The spectrum of ionospheric irregularities are shown to follow the power law (Yeh and Liu, 1982). The slope of this spectrum is the spectral index, and is often determined using high rate

data. In the absence of the high rate data like for our case, the spectral slope was estimated from the low rate C/NOFS ion density data. A typical spectrum computed using FFT for orbit 18348 is shown in Figure 7 a. The straight line is the least square fit to the spectrum on log-log

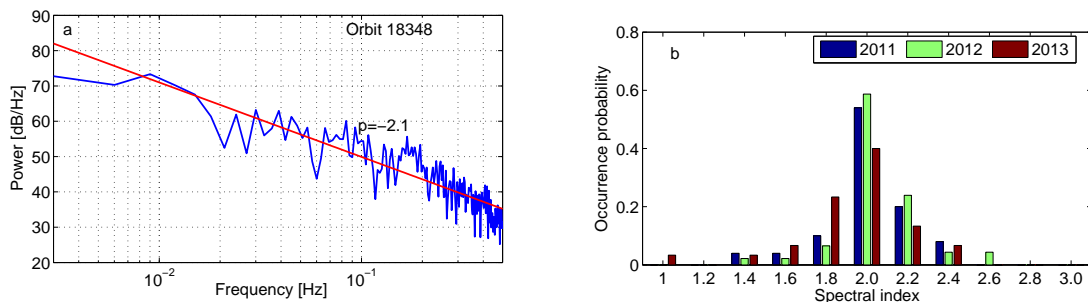


Figure 7: (a) Power spectral density of the 1 s ion density data between 23.00-23:25 LT for orbit 18348 on 2011-09-03. A spectral slope of 2.1 was obtained. (b) The distribution of the slope of the linear fit to the power spectral density function on log-log scale

scale, and the slope of this line is the in-situ spectral index. To determine the optimum spectral index, slopes of the power spectra for the ion density irregularities observed over East Africa were determined. Figure 7 b shows the distribution of the occurrence of the in-situ spectral indices in bins of 0.2. Spectral indices between 2.0-2.2 had the highest occurrence during the period of study. The occurrence rate decreased for spectral indices below or above the range 2.0-2.2. Similar results were obtained by Patel *et al.* (2011) using Stretched Rohini Satellite Series C2 (SROSS-C2) data, in which spectral slope of 2.0 had the maximum occurrence rate. To estimate the phase spectral index which we used in Equation 3, we added 1 to the optimum value of the in-situ spectral index. The estimated zonal irregularity drifts using this index are presented in the section below.

### 3.3.2. Irregularity drift velocity from scintillation indices

A proposed method to estimate zonal irregularity drifts from scintillation indices (Carrano *et al.*, 2016) was used in this study. To distinguish scintillation phenomena from other noise effects, and to remain within the weak scatter assumption, only  $S_4$  values between 0.2-0.6 and  $\sigma_\phi$  between 0.05-1.0 radians were used. The magnetic field angles in Equation 2 were computed using MATLAB IGRF codes written by Rino<sup>2</sup>. We calculated zonal drift velocities for all scintillating satellites with elevation greater than 30°. The zonal drift velocities from the different satellites were averaged over five minutes and the results are shown in Figure 8. To compare the zonal drifts from the SCINDA receivers with those from C/NOFS IDM, five minute average zonal ion drifts from C/NOFS satellite are included in Figure 8 c, d and e. Since the IDM works better in an environment rich of both heavy and lighter ions (Coley *et al.*, 2014), only data for which the ion fraction was between 0.4-0.9 for satellite passes over East Africa between 18:00-03:00 LT were considered. In Figure 8 a, b and f, C/NOFS data did not meet our set criteria.

From Figure 8 a, both VHF and L-band scintillations were observed over Nairobi with the VHF scintillation lasting longer than the L band scintillation. The peak zonal drift velocity derived from the VHF receiver at Nairobi on Day Of the Year (DOY) 161 in 2011 was about 80.0 m s<sup>-1</sup> at about 22:00 LT which reduced gradually to about 45.0 m s<sup>-1</sup> at 1:00 LT. The zonal irregularity drift velocity estimated from the scintillating PRNs on the same day had a peak of about 100.0 m s<sup>-1</sup>. On DOY 215 in 2011, VHF scintillation was also observed to last longer than the L-band scintillations (Figure 8 b). The peak zonal drift velocity from the VHF

<sup>2</sup><https://www.mathworks.com/matlabcentral/fileexchange/28874-igrf-magnetic-field>

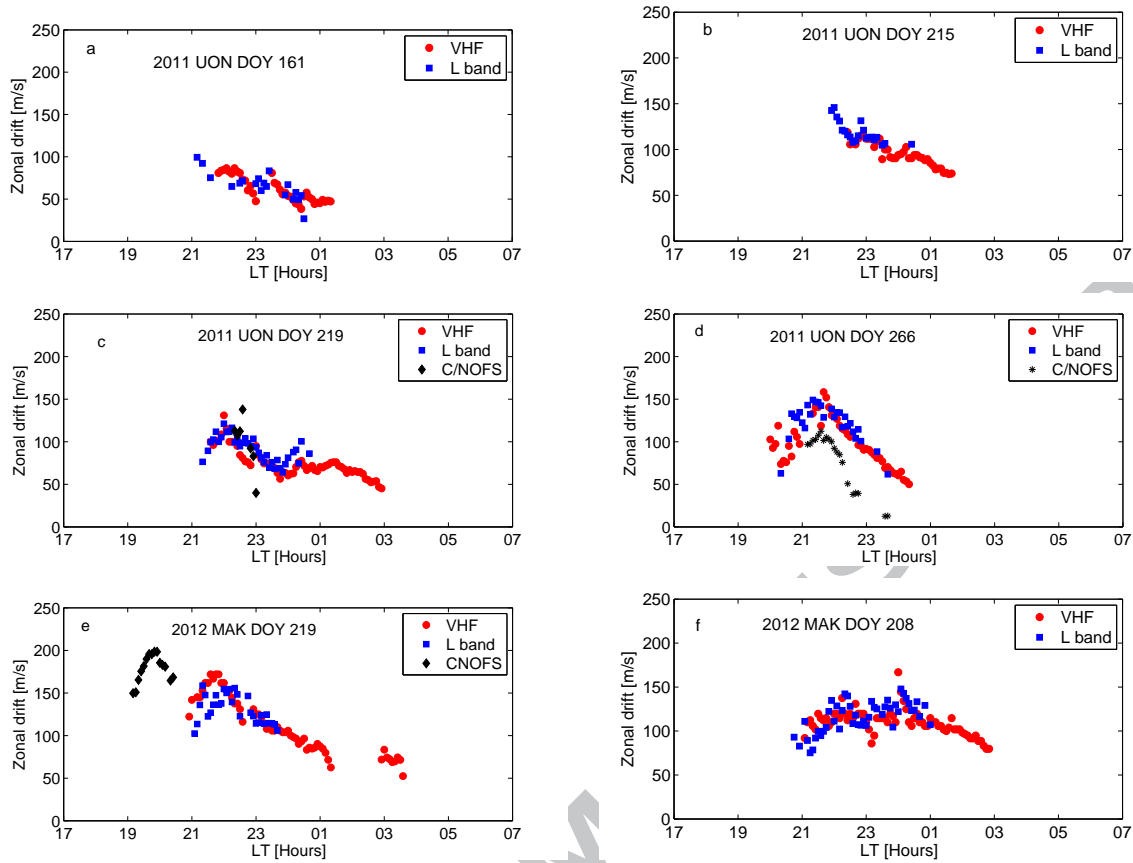


Figure 8: Comparison between the five minute mean zonal drift velocities from L-band scintillation indices, VHF receivers and C/NOFS ion drift meter

at Nairobi was about  $120 \text{ m s}^{-1}$  at about 21:30 LT. The zonal drift velocity estimate from the GPS-SCINDA at Nairobi on the same day had a peak of about  $140 \text{ m s}^{-1}$  at about 22:00 LT. In Figure 8 c, both VHF scintillation and L-band scintillation started at about the same time, though VHF scintillation lasted for a longer time. The zonal drift velocity estimates from the VHF and the GPS-SCINDA at Nairobi were about  $125 \text{ m s}^{-1}$  and  $120 \text{ m s}^{-1}$  respectively. On the same evening, C/NOFS satellite passed over the longitude region and the average zonal ion drift velocity from the IDM was about  $100 \text{ m s}^{-1}$ . Another case of both VHF and L band scintillation occurring simultaneously, and C/NOFS satellite passing over East Africa was on DOY 266 in 2011 at UON (Figure 8 d). The zonal drifts from the IDM were generally lower than the zonal drifts derived from VHF and GPS-SCINDA receivers on the same day. On DOY 219 in 2012, C/NOFS satellite crossed the longitude region at about 19:00-20:00 LT and the zonal drift from the IDM was about  $150\text{-}200 \text{ m s}^{-1}$ . While VHF and L band scintillations started at about 21:00 LT and the maximum drift from the VHF and the GPS-SCINDA at Makerere were about  $175 \text{ m s}^{-1}$  and  $160 \text{ m s}^{-1}$  respectively. The differences in the zonal drift velocities from the SCINDA receivers with those from the IDM could be due to changes in relative magnitude of the mechanisms that result in the zonal motions at the different altitudes. Figure 8 a, b, c and d show that the zonal drift velocity estimates from the L-band scintillation indices derived from the Nairobi GPS-SCINDA for these days were comparatively similar to the zonal drift velocity estimates from the co-located VHF at Nairobi. Similarly, the zonal drift velocity estimates from the L-band scintillation indices derived from the GPS-SCINDA at Makerere in 2012 were also in good agreement with the zonal drift velocities from the VHF receiver at Makerere (Figure 8 e and f). Important to note here is that no cases of  $S_4$  passing our selection criterion were observed after 01:00 LT in order to compare the late night zonal irregularity drift velocities which in most cases are generally low. The prolonged VHF scintillation observed in this study

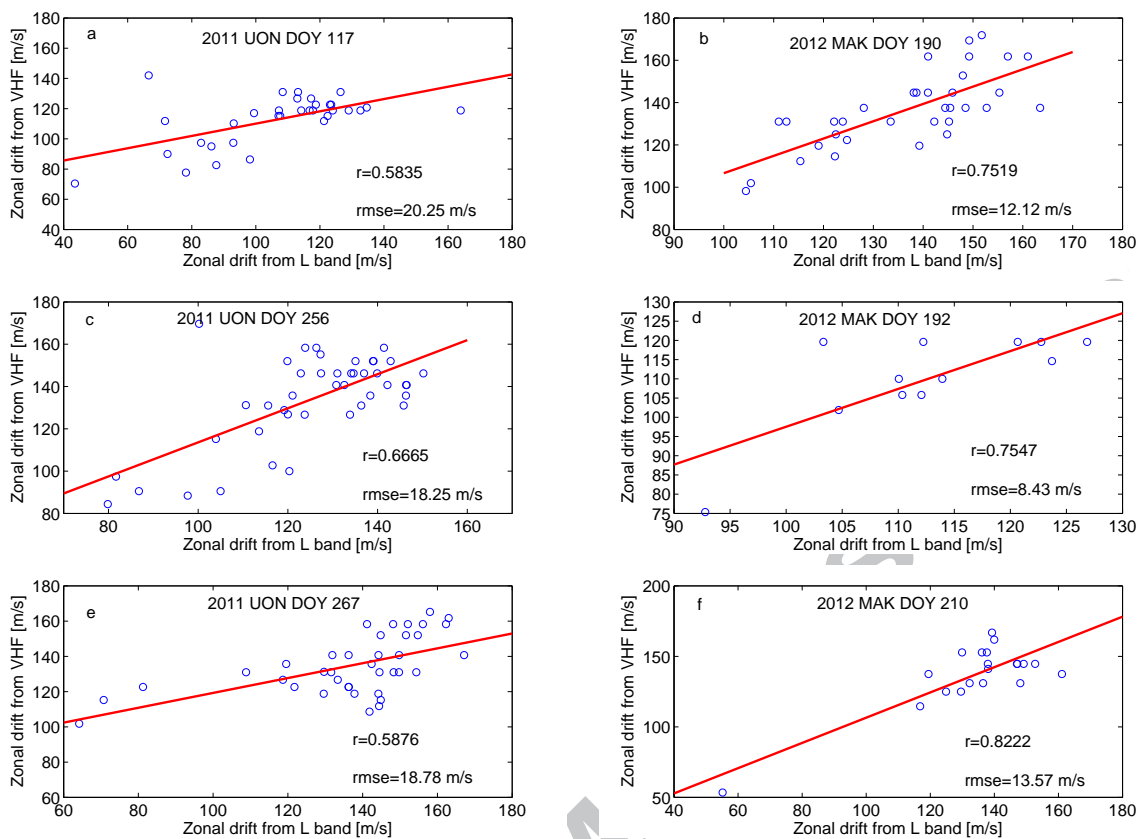


Figure 9: Correlation analysis of five minute mean zonal drift velocities derived from L-band scintillation indices with those derived from co-located VHF receivers.  $r$  is the Pearson linear correlation coefficient and  $rmse$  is the mean square error

is consistent with results from similar studies (Rao *et al.*, 2005; Olwendo *et al.*, 2013) over the low latitude region. These post midnight scintillations are attributed to large scale irregularities of bottomside sinusoidal type which often extend past midnight (Rao *et al.*, 2005).

To further study the suitability of the L-band scintillation indices in estimating the zonal irregularity drift velocities over East Africa, the daily drift velocities from the VHF and GPS-SCINDA corresponding to the same time were compared. We used the five minute average drift velocities to determine the correlation coefficient between the two data sets. Figure 9 shows the results for some events at UON in 2011 and at MAK in 2012. A positive correlation ( $r \sim 0.58-0.67$ ) was observed between the zonal drift velocities from UON GPS-SCINDA receiver and the zonal drift velocities from the VHF receiver at Nairobi on DOY 117, 256 and 267 in 2011 (Figure 9 a, c and e). A similar positive ( $r \sim 0.75-0.82$ ) correlation between zonal drift velocity estimates from GPS-SCINDA at MAK and zonal drift velocity from the VHF at Makerere was also observed on DOY 190, 192 and 210 in 2012 (Figure 9 b, d and f). These zonal drift velocity estimates had root mean square error of about 12.0-20.0 m/s between the GPS-SCINDA estimated drifts and those from the VHF. Though cases of deviation were observed, the results in this study support the method proposed by Carrano *et al.* (2016) to estimate the zonal irregularity drift velocities from L-band scintillation indices.

#### 4. Conclusion

We used three years data from C/NOFS satellite to characterize plasma density irregularities during increasing solar activity period 2011-2013. Several ion density irregularities were observed in C/NOFS data throughout the years studied. These ion density irregularities were majorly a nighttime phenomena with peak occurrence time between 20:00-00:00 LT. The ion

density irregularities were observed to occur mainly at lower altitudes, and the occurrence probabilities reduced significantly as the altitude increased. Longitudinal variations of ion density irregularities showed maximum occurrence probability at about 270-300°E followed by 135-180°E and 0-30°E. Analysis of the C/NOFS zonal ion drifts revealed that the strongest nighttime drifts were in 270-300°E followed by 0-30°E longitude sectors. An estimate of the spectral slope for the plasma density irregularities from the in-situ data showed broad values with a modal value of 2.0-2.2. A positive correlation with correlation coefficients of  $\sim 0.58$ -0.82 was found between the zonal irregularity drift velocities estimated from L-band scintillation indices and the zonal irregularity drift velocities derived from co-located VHF receivers in East Africa. The nighttime zonal ion drift velocities from C/NOFS IDM in 30-60°E longitude region are generally in the same range (100-150 m s<sup>-1</sup>) (Figure 6) with peak zonal irregularity drift velocities from SCINDA receivers in East Africa. The differences observed in the few cases in Figure 8 are possibly due to variations in the relative magnitude of the seed mechanisms that drive the zonal ion motions at the different altitudes.

### Acknowledgement

Financial support from International Science Programme (ISP) of Uppsala University in Sweden. We are thankfully to AFRL, USA for supplying the GPS-SCINDA receivers used in this study. The authors acknowledge the two anonymous reviewers for their constructive comments and suggestions.

### References

- Abdu M.A., Bittencourt J.A. and Batista I.S., 1981. Magnetic declination control of the equatorial f region dynamo electric field development and spread F. *J. Geophys. Res.* 86, pp. 11443–11446.
- Beaujardière O.D.L., Jeong L. and the C/NOFS Science Definition Team., 2004. C/NOFS: A Mission to Forecast Scintillations. *J. Atmos. Sol.-Terr. and Planetary Sci.*, 66, pp. 1573–1591.
- Burrell A.G., Heelis R.A. and Stoneback R.A., 2012. Equatorial longitude and local time variations of topside magnetic field-aligned ion drifts at solar minimum. *J. Geophys. Res.* 117, p. A04304.
- Carrano C.S., Groves K.M., Rino C.L. and Doherty P.H., 2016. A technique for inferring zonal irregularity drift from single station GNSS measurements of intensity ( $S_4$ ) and phase ( $\sigma_\phi$ ) scintillations. *Radio Sci.* 51, doi:10.1002/2015RS005864.
- Coley W.R. and Heelis R.A., 1994. Comparison of low-latitude ion and neutral zonal drifts using DE 2 data. *J. Geophys. Res.* 99, pp. 341–348.
- Coley W.R., Stoneback R.A., Heelis R.A. and Hairston M.R., 2014. Topside equatorial zonal ion velocities measured by C/NOFS during rising solar activity. *Ann. Geophys.* 32, pp. 69–75.
- de Kamp M.M.J.L.V. and Cannon P.S., 2009. Spectra of equatorial total electron content derived from GPS signals. *Ann. Geophys.* 27, pp. 2205–2214.
- Fejer B.G., de Paula E.R., Gonzalez S.A. and Woodman R.F., 1991. Average vertical and zonal F region plasma drifts over Jicamarca. *J. Geophys. Res.* 96, pp. 13901–13906.
- Fejer B.G., Kudeki E. and Farley D.T., 1985. Equatorial F region zonal plasma drifts. *J. Geophys. Res.* 90, pp. 12249–12255.

- Fejer B.G., Tracy B.D. and Pfaff R.F., 2013. Equatorial zonal plasma drifts measured by the C/NOFS satellite during the 2008-2011 solar minimum. *J. Geophys. Res.* 118, pp. 3891–3897.
- Haerendel G., 1973. Theory of equatorial spread F. Maxplanck Institute fur Extra Terrestridie Physik.
- Heelis R., 2004. Electrodynamics in the low and middle latitude ionosphere: A tutorial. *J. Atmos. Sol.-Terr.* 66, p. 825–838.
- Huang C.Y., Burke W.J., Machuzak J.S. and Sultan P.J., 2001. DMSP observations of equatorial plasma bubbles in the topside ionosphere near solar maximum. *J. Geophys. Res.* 106, pp. 8131–8142.
- Huang C., Rich F.J., de La Beaujardiere O. and Heelis R.A., 2010. Longitudinal and seasonal variations of the equatorial ionospheric ion density and eastward drift velocity in the dusk sector. *J. Geophys. Res.* 115, p. A02305.
- Hysell D.L. and Burcham J.D., 1998. JULIA radar studies of equatorial spread F. *J. Geophys. Res.* 103, pp. 29155–29167.
- Immel T.J., Frey H.U., Mende S.B. and Sagawa E., 2004. Global observations of the zonal drift speed of equatorial ionospheric plasma bubbles. *Ann. Geophys.* 22, pp. 3099–3107.
- Jensen J.W. and Fejer B.G., 2007. Longitudinal dependence of middle and low latitude zonal plasma drifts measured by DE-2. *Ann. Geophys.* 25, pp. 2551–2559.
- Ji S., Chen W., Ding X. and Zhao C., 2011. Equatorial ionospheric zonal drift by monitoring local GPS reference networks. *J. Geophys. Res.* 116, p. A08310.
- Kelley M.C., 2009. The Earth's ionosphere: Plasma Physics and Electrodynamics. Amsterdam academic Press, second edition.
- Kil H. and Heelis R.A., 1998. Global distribution of density irregularities in the equatorial ionosphere. *J. Geophys. Res.* 103, pp. 407–417.
- Kintner P.M., Ledvina B.M., de Paula E.R. and Kantor I.J., 2004. Size, shape, orientation, speed, and duration of GPS equatorial anomaly scintillations. *Radio Sci.* 39, p. RS2012.
- Ledvina B.M., Kintner P.M. and de Paula E.R., 2004. Understanding spaced-receiver zonal velocity estimation. *J. Geophys. Res.* 109, p. A10306.
- Liu Y.H., Liu C.H. and Su S.Y., 2012. Global and Seasonal Scintillation Morphology in the Equatorial Region Derived from ROCSAT-1 In-situ Data. *Terr. Atmos. Ocean Sci.* 23, pp. 95–106.
- Maruyama T. and Matuura N., 1984. Longitudinal Variability of Annual Changes in Activity of Equatorial Spread F and Plasma Bubbles. *J. Geophys. Res.* 89, pp. 10903–10912.
- Nade D.P., Sharma A.K., Nikte S.S., Patil P.T., Ghodpage R.N., Rokade M.V., Gurubaran S., Taori A. and Sahai Y., 2013. Zonal velocity of the equatorial plasma bubbles over Kolhapur, India. *Ann. Geophys.* 31, pp. 2077–2084.
- Olwendo O., Baluku T., Baki P., Cilliers P., Mito C. and Doherty P., 2013. Low latitude ionospheric scintillation and zonal irregularity drifts observed with GPS-SCINDA system and closely spaced VHF receivers in Kenya. *Adv. Space Res.* 51, pp. 1715–1726.

- Patel K., Singh A.K., Subrahmanyam P. and Singh A., 2011. Modeling of ionospheric scintillation at low-latitude. *Adv. space Res.* 47, pp. 515–524.
- Rao P.V.S.R., Ram S.T., Niranjana K., Prasad D.S.V.V.D., Krishna S.G. and Lakshmi N.K.M., 2005. VHF and L-band scintillation characteristics over Indian low latitude station, Waltair (17.7°N, 83.3°E). *Ann. Geophys.* 23, pp. 2457–2464.
- Richmond A.D. and Roble R.G., 1997. Electrodynamic coupling effects in the thermosphere/ionosphere system. *Adv. Space Res.* 20, pp. 1115–1124.
- Rino C.L., 1979. A power law phase screen model for ionospheric scintillation: 1. weak scatter. *Radio Sci.* 14, pp. 1135–1145.
- Rodrigues F.S., Crowley G., Azeem S.M.I. and Heelis R.A., 2011. C/NOFS observations of the equatorial ionospheric electric field response to the 2009 major sudden stratospheric warming event. *J. Geophys. Res.* 116, p. A09316.
- Stoneback R.A., Heelis R.A., Burrell A.G., Coley W.R., Fejer B.G. and Pacheco E., 2011. Observations of quiet time vertical ion drift in the equatorial ionosphere during the solar minimum period of 2009. *J. Geophys. Res.* 116, p. A12327.
- Su S., Liu C.H., Ho H.H. and Chao C.K., 2006. Distribution characteristics of topside ionospheric density irregularities: Equatorial versus midlatitude regions. *J. Geophys. Res.* 111, p. A06305.
- Van Dierendonck A.J., Klobuchar J.A. and Hua Q., 1993. Ionospheric scintillation monitoring using commercial single frequency C/A code receivers. paper presented at Institute of Navigation GPS-93 in September 1993.
- Yeh K.C. and Liu C.H., 1982. Radio Wave Scintillations in the Ionosphere. *Proc. IEEE.* 70, pp. 324–360.